Automatic Alignment of Histological Sections for 3D Reconstruction and Analysis

Sébastien Ourselin, Alexis Roche, Gérard Subsol, Xavier Pennec, Christophe Sattonnet

INRIA

INSTITUT NATIONAL DE RECHERCHE EN INFORMATIQUE ET EN AUTOMATIQUE

Automatic Alignment of Histological Sections for 3D Reconstruction and Analysis

Sébastien Ourselin, Alexis Roche, Gérard Subsol, Xavier Pennec, and Christophe Sattonnet

N° 3595

Décembre 1998

THÈME 3

ISSN 0249-6399

INRIA
SOPHIA ANTIPOLIS

Automatic Alignment of Histological Sections for 3D Reconstruction and Analysis

Sébastien Ourselin*, Alexis Roche, Gérard Subsol, Xavier Pennec, and Christophe Sattonnet†

Thème 3 — Interaction homme-machine,
images, données, connaissances
Projet Epidaure

Rapport de recherche n° 3595 — Décembre 1998 — 27 pages

Abstract: In this report, we present a new method of aligning histological sections. First a displacement field between the two images is computed by block matching. Then we estimate a rigid transformation based on the field. The process is integrated within a multi-scale scheme. We carefully study the problem of robustness and we propose several ideas to deal with inter-section intensity differences and background artifacts. We demonstrate experimentally that we can reach a sub-voxel accuracy and we show some results on histological sections of a rat's brain and an endometrical adenocarcinoma.

Key-words: histological sections, registration, robust estimation, block matching

* Email: Sebastien.Ourselin@sophia.inria.fr
† Anatomo-pathology Laboratory, 31 ter, boulevard Maréchal Juin - 06800 Cagnes-sur-Mer - France

Unité de recherche INRIA Sophia Antipolis
2004, route des Lucioles, B.P. 93, 06902 Sophia Antipolis Cedex (France)
Téléphone : 04 92 38 77 77 - International : +33 4 92 38 77 77 — Fax : 04 92 38 77 65 - International : +33 4 92 38 77 65

Alignement automatique de coupes histologiques pour la reconstruction et l'analyse tridimensionnelles

Résumé : Dans ce rapport, nous présentons une nouvelle méthode d'alignement de coupes histologiques. Tout d'abord, nous calculons un champ de déplacement entre deux images par une technique de mise en correspondance par blocs. Puis, nous estimons une transformation rigide à l'aide de ce champ. L'ensemble de cette méthode est intégré dans un processus multi-échelle. Nous nous intéressons au problème de la robustesse et nous montrons expérimentalement que cette méthode permet d'atteindre une précision inférieure au voxel. Nous présenterons enfin quelques résultats d'alignement de coupes de cerveau de rat et d'un adenocarcinome de l'endomètre.

Mots-clés : coupes histologiques, recalage, estimation robuste, mise en correspondance par blocs

Contents

1 Introduction

1.1 Presentation of the problem

Histological sections provide useful and additional information to 3D medical images for the diagnosis or the study of pathology. To obtain histological sections, the anatomical structure is first fixed using paraffin embedding or by cryogenisation. Then it is trimmed into thin sections with a constant inter-section gap. The sections are laid on a microscope cover-glass where they can be stained according to the sub-structures we want to emphasize. The microscopic images are then scanned using a digital camera.

The whole process is performed independently for each section. So, there is no alignment between the different images as we can see in Figure 1. Whereas we begin with a real 3D block of data, we obtain at the end a set of 2D data that are no longer spatially correlated. In order to perform a 3D analysis of the anatomical structure, we need to **register** the sections to recover the original alignment.

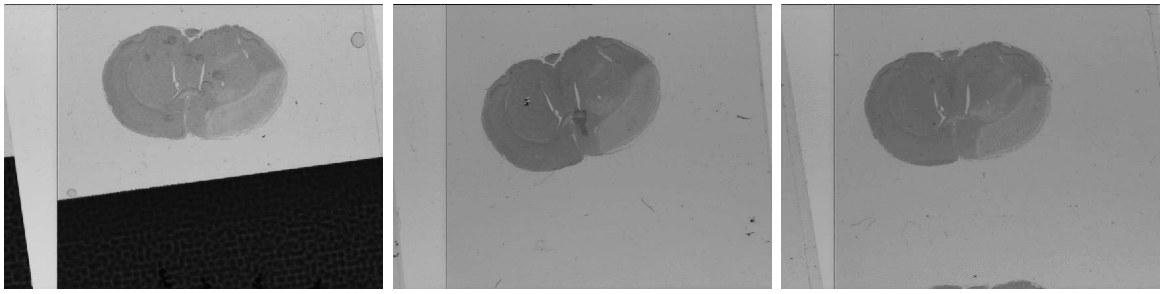

Figure 1: *Three consecutive stained rat's brain histological sections. We can see how they are misaligned.*

1.2 Difficulties of the problem

With average quality data which can be obtained in current laboratory, we find different problems.

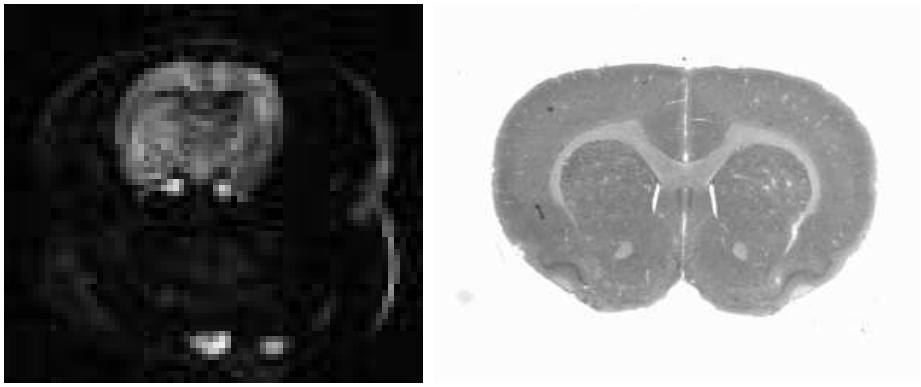

Figure 2: *Left: a MRI slice of rat's brain with a resolution of* 72×65 *pixels (*$0.47 \times 0.47mm$*), and an inter-section gap of* $1mm$*. Right: a histological section of a rat's brain with a resolution of* 768×576 *pixels (*$0.03 \times 0.03mm$*) and an inter-section gap of* $0.4mm$*.*

First, in the following examples, the digitized images have a resolution of 768×576 pixels, 7 times larger than a typical MR slice (see Figure 1). Moreover, if they are in color with Red, Green, Blue components encoded in 1 byte, the section image is 21 (7×3) times larger.

When laying the sample on the cover-glass some spots can appear and the edges of the cover-glass can be in the field of view of the camera (as in the example of Figure 1). All this can create a lot of artifacts in the background.

The staining process is performed independently for each section. Thus, the intensity contrast can be different. Moreover, a change of lighting can occur during the digitalization of the sections. This leads to a difference of global intensity from one section to an other.

During sectioning, the edges of the sections can be distorted or even torn out. This can prevent the use of edges as reliable landmarks. More generally, during sectioning, the whole section can be deformed. Nevertheless, we will assume in the following that the distortions remain small enough to assume that the transformation between two consecutive sections is rigid, *i.e.* the composition of a rotation (one angle parameter) and a translation (two parameters).

Two successive sections are all the more different as the inter-section gap is large. In fact, the intrinsic problem of section registration remains the fact that we have to find a rigid transformation whereas the two sections are not exactly the same. Moreover, between two consecutive sections, we can have very large translations and rotations that can reach half the field of view or 90 degrees.

From all these observations, we conclude that a section registration method should be:

- **Fast** enough to deal with several tens of section registration in a reasonable time in spite of the large quantity of information.
- **Robust with respect to background artifacts.** Most of them can be deleted by a simple preprocessing, but some of them, like spots or marks, could remain.
- **Insensitive to inter-section variation of intensity.** This is a very important point in dealing with the stained sections that give a lot of information.
- **Robust with respect to the initial conditions**, to be able to recover large displacements.
- **Not based on external edges**. Often, with the histological sections, edge features are unreliable or cannot deal with precise registration. Moreover, the position of point features can also be shifted due to the geometrical distortions.
- **Accurate** to be able to use the accuracy of the histological sections. Nevertheless, it is very difficult to estimate the precision of the result. Indeed, even with a perfect registration, *i.e.* that corresponds to the position before cutting, no criterion will be equal to zero since two consecutive sections are not identical.

1.3 A brief survey on sections registration

We can classify existing sections registration methods into four kinds:

- **Manual methods.** The user aligns the sections interactively [DSC+93]. It is a non reproducible method because it is user-dependent and it is based on the structure the user want to focus on. Moreover, it is a tremendous task and it cannot be used with a large number of sections.

- **Fiducial markers based methods.** In general, fiducial markers consist of holes which are created by the track of needles stuck in the structure block before cutting [GTH+95]. We have seen that geometrical distortions can shift these point landmarks and then blur the registration accuracy. Moreover, creating fiducial markers can destroy a part of the structure and then prevent any *post-mortem* diagnosis. Such a method can be used for a 3D reconstruction of an anatomical structure but not for any image processing which should lead to clinical conclusions.

- **Feature based methods.** This kind of method requires first the extraction of some features (points, lines, regions) from the image. We can first segment the section in two successive sections, compute the principal axes of the segmented mask and align the axes. In [HH88], this alignment is considered sufficient for the histological sections. But the precision remains very limited (see [SZ97]). It is also possible to match either the contours of the section [ZYG93, Dum96, CYHN98] or the edges [KFM+95, KRBC96]. This can be done with methods based on Chamfer distance [KRBC96], disparity analysis [ZYG93], B-spline decomposition [CYHN98] or gray scale edge image correlation [KFM+95]. In [RCM+97], point features are extracted in autoradiographs and are matched with Robust Point Matching method.

- **Iconic method**. There is no feature extraction as the matching algorithm takes into account the intensities of the whole image. We can cite the algorithms based on intensity correlation [ADAL92] or mutual information [KBFM97].

1.4 Discussion and overview of the paper

One requirement for the method is not to use edges as they could be unreliable. Nevertheless, global iconic methods that deal with the whole image are very

sensitive to the contiguous section differences. We propose then to use a local iconic method that determine a local displacement field based on intensity similarity on small sub-blocks of the image. Then, we gather all this local information to define a general rigid transformation of the image. One key-point of the transformation computation is the robustness. So, we have first to choose a similarity measure that takes into account the inter-section variation in intensity. Secondly, to deal with the contiguous section differences and the background artifacts, we have to introduce a robust estimation method of the transformation. In order to accelerate the process, to deal with large displacement and to obtain accurate results, we develop a multi-scale scheme.

In section 2, we present the new algorithm and we describe precisely all its steps. In section 3, we analyze quantitatively the robustness with respect to the relative displacement of the two sections. In section 4, we present some applications. In particular, we point out how the 3D homogeneity allows performance of a more precise segmentation of some structures. In the last section, we propose several research tracks for future work.

2 Description of the algorithm

2.1 General presentation

The algorithm takes as its input two section images: reference image I_1 and a floating image I_2 that have the same size (X lines and Y columns. The result will be the rigid transformation T and the image $I = I_2 \circ T^{-1}$ which is aligned with I_1.

The algorithm follows an iterative scheme (see Figure 3) which computes at each step a global vector field between the current floating image I and I_1 and estimates a rigid transformation S which is composed with the current rigid transformation T. Then a new current floating image I is obtained by resampling I_2 with T. Notice that there is only one resampling to compute I, which limits the loss of information. Depending on δ which characterizes the « magnitude » of S, some parameters are modified and the process is iterated.

2.2 Computing a displacement field

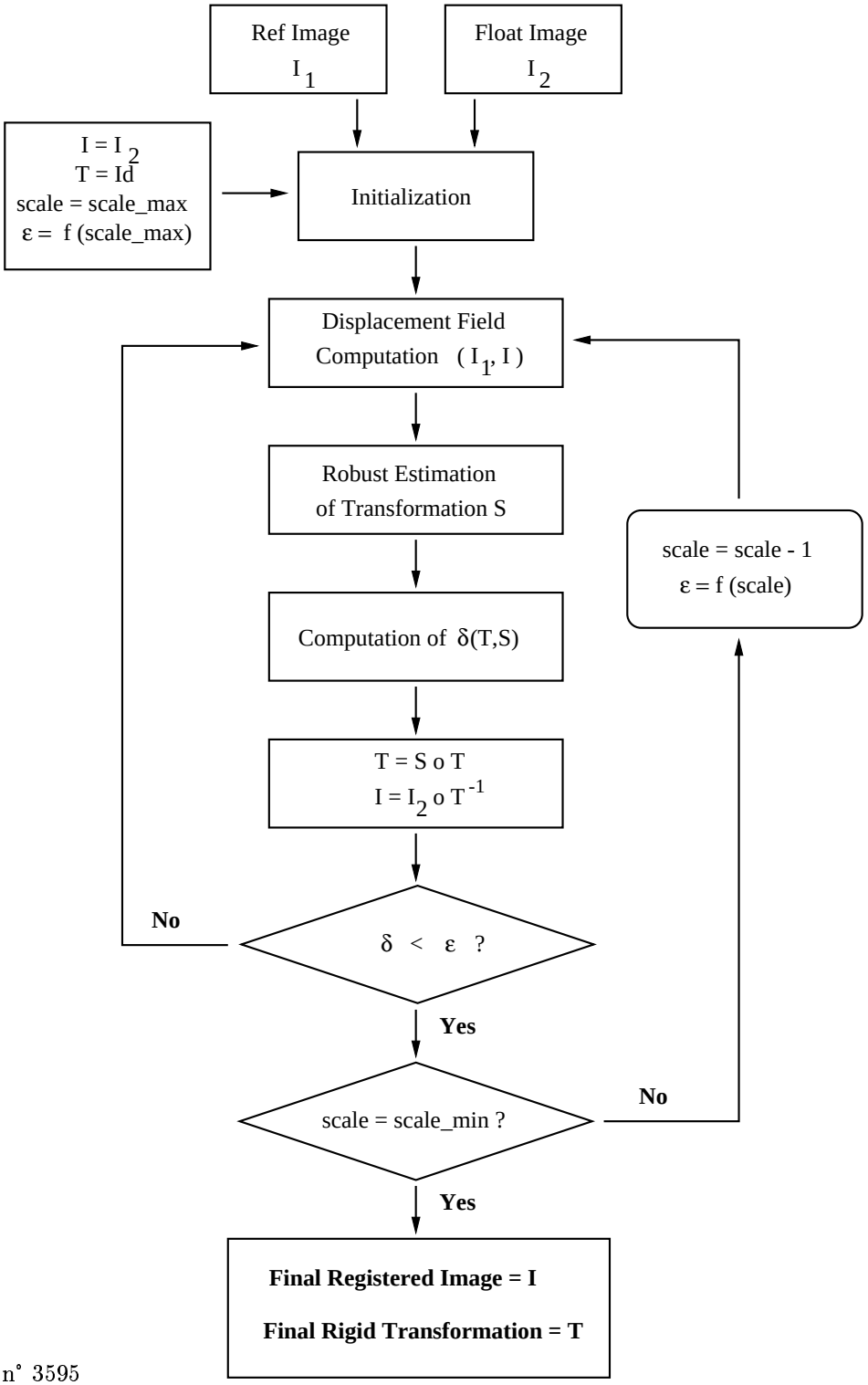

Figure 3: *The different steps of the algorithm.*

2.2.1 The Block Matching scheme

The *Block Matching* scheme has similarities with image compression methods such as MPEG II [BK97]. Compression algorithms make a movement compensation between two successive images by finding the displacement of luminance blocks. The idea is to move a block $\mathcal{B}$ of the first image in its neighborhood and to compare it to the blocks $\mathcal{B}'$ that have similar positions in the second image. The best corresponding block $\mathcal{B}'$ allows the definition of a vector between the centers of blocks $\mathcal{B}$ and $\mathcal{B}'$ which determines a local displacement between the two images (see Figure 4).

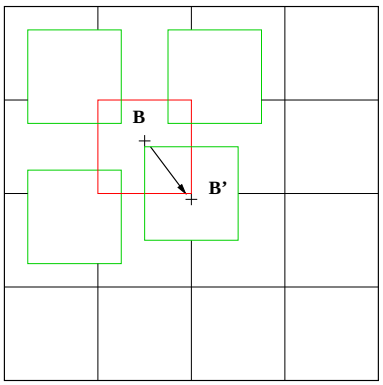

Figure 4: *The block $\mathcal{B}$ (in red) of first image is moved around its initial position (green positions) and compared to the blocks $\mathcal{B}'$ that have similar position in the second image. The best corresponding block $\mathcal{B}'$ allows to define a vector between the centers of blocks $\mathcal{B}$ and $\mathcal{B}'$ that determine to a local displacement between the two images.*

More precisely, in our application, the first image is the current floating image I and the second image is the reference image I_1. Let $\mathcal{B}_{ij}$ (resp. $\mathcal{B}'_{ij}$) a block of $N \times N$ dimension of image I (resp. I_1), where (i, j) are the coordinates of the left up corner of this block.

- for $(i = 0 \ ; \ i \leq X - N \ ; \ i = i + \Delta_1)$
- for $(j = 0 \ ; \ j \leq Y - N \ ; \ j = j + \Delta_1)$

- For the block $\mathcal{B}_{ij}$ of image I_1:
  - for $(k = i - N \ ; \ k \leq i + N \ ; \ k = k + \Delta_2)$
  - for $(l = j - N \ ; \ l \leq j + N \ ; \ l = l + \Delta_2)$
  - Compute the value $\mathbf{C}_{ij}^{k,l}$ of a similarity measure between $\mathcal{B}_{ij}$ and $\mathcal{B}'_{kl}$.
- Let $\mathcal{B}'_{mn} = argmax \mathbf{C}_{ij}^{k,l}$ the block that maximizes the value of the similarity measure. It defines the displacement vector between $(i + N/2, j + N/2)$ and $(m + N/2, n + N/2)$.

The list of displacement vectors define a displacement field $\mathcal{D}_{I \to I_1}$ that approximates the transformation between I and I_1. Notice that the number of vectors of $\mathcal{D}_{I \to I_1}$ depends on the block step Δ_1 that must be lower than the block size N to take into account all the image pixels. Thus, Δ_1 defines the *displacement field resolution.*

With a block size of N, we can find a maximal displacement vector of N pixels (more precisely, $\sqrt{2}N$ in the corner as we choose a squared neighborhood). So N can be considered as a *transformation scale parameter.*

The number of comparison tests to find the best similar block is: $\left(\frac{2N}{\Delta_2}\right)^2$. Thus, Δ_2 is an indicator of the *accuracy* of the matching process.

2.2.2 An intensity similarity measure: the correlation coefficient

Many similarity measures have been proposed for image registration [PWL+98] (sum of squared differences, correlation, mutual information [MCV+97, Vio97], correlation ratio [RMPA98]...). Choosing a particular measure must depend on the kind of relation which can be assumed between intensities of the registered images.

If we assume that the blocks to be registered are affinely correlated, there exist two local constants α and β such that $I(i,j) \approx \alpha\, I_1(i+m, j+n) + \beta$ where $I(i,j)$ and $I_1(i+m, j+n)$ denote the intensity of the pixels with coordinates (i,j) in image I and $(i+m, j+n)$ in image I_1, respectively. This relation is considered valid only if the blocks are registered (i.e. if m and n are the correct translational parameters), and if the pixel coordinates are taken *inside*

the blocks. Therefore, this model allows us to take into account an inter-section bias which is locally affine.

It has been proved by several authors (see [Bro92]) that a similarity measure adapted to affine models is the *correlation coefficient* (sometimes also called normalized cross correlation). We recall now its definition.

Let $\overline{I}_{(a,b)}$ and $\overline{I}_{1(u,v)}$ be the means of I on block $\mathcal{B}_{ab}$, and I_1 on block $\mathcal{B}'_{uv}$, respectively, and let $\sigma_I(a,b)$ and $\sigma_{I_1}(u,v)$ be the corresponding standard deviations. Then, the correlation coefficient between the blocks $\mathcal{B}_{ab}$ and $\mathcal{B}'_{uv}$ is given by :

$$\mathbf{C}(\mathcal{B}_{ab},\mathcal{B}'_{uv}) = \frac{1}{N^2}\sum_{i=0}^{N-1}\sum_{j=0}^{N-1}\frac{\left[I(a+i,b+j)-\overline{I}_{(a,b)}\right]\ \left[I_1(u+i,v+j)-\overline{I}_{1(u,v)}\right]}{\sigma_I(a,b)\,\sigma_{I_1}(u,v)}. \tag{1}$$

It is important to emphasize that $\mathbf{C}$ has a low cost calculation with respect to other measures such as mutual information. This is critical in our algorithm because each block correspondent is found through an exhaustive research in the block neighborhood. Thus, numerous evaluations of the similarity measure are needed, which can be done with reasonable computing time using the correlation coefficient.

However, as shown in [LM95], $\mathbf{C}$ is not reliable in the presence of occlusions (e.g. background artifacts). This is to say that the matching between two blocks may be bad if one of them surrounds an occlusion. This is why we have to introduce a robust approach for estimating the rigid transformation based on the displacement field.

2.3 Computing a robust estimation of the rigid transformation

The block matching step described in section 2.2.1 provides a list of corresponding 2D points, x_k and y_k, denoting the centers of the matched blocks. We can interpret the data-points $(x_k, y_k - x_k)$ as an approximate sampling of the actual rigid displacement field which maps I to I_1. The problem we address now is to estimate the 3 parameters of this rigid transformation, that is find a rotation angle θ (or, equivalently, a two-by-two rotation matrix R) and a translation vector $t = (t_1, t_2)$.

Given arbitrary R and t, let us define the residuals as the 2D vectors

$$r_k = y_k - Rx_k - t.$$

The problem can then be formulated as minimizing some cost function of the residuals with respect to R and t. A classical choice is the sum of the Euclidean norm of the squared residuals, yielding a least square (LS) estimator :

$$\min_{R,t} \sum_k \|r_k\|^2. \tag{2}$$

The LS approach has several advantages. Notably, its solution is unique and explicit (several closed forms and algorithms are discussed in [ELF97]). However, it is well-known that LS is not robust in the sense that outlying displacements may strongly perturbate the result. In our case, due to the numerous image artifacts, it may happen that some blocks in I have bad correspondences in I_1 (in our experiments, typically 20% of the blocks).

Various studies, carried out in analogous rigid estimation problems [ZDFL94, SB97], have shown that M-estimators techniques can provide solutions which are robust to such bad locations. As explained in [RL87], M-estimators generalize LS by replacing the squared residuals $\|r_k\|^2$ in equation (2) with another function, yielding

$$\min_{R,t} \sum_k \rho(\|r_k\|),$$

where ρ is a symmetric, positive-definite function with a unique minimum at zero[1]. The basic idea is to reduce the influence of outliers by choosing a slowly increasing function ρ.

Several forms have been proposed for ρ, but many of them depend on a tuning parameter c, often called the *cut-off distance*. Roughly speaking, c represents the threshold beside which a residual is discarded. Tuning c suitably is critical since it rules the trade-off between robustness (discard outlying data) and accuracy (take into account as much good data as possible). Therefore, c has itself to be estimated in a robust way, which requires in practice a good initialization of R and t.

[1] In fact, this definition of M-estimators is restrictive in the multidimensional case [RL87]

Some non-parametric M-estimators are robust while reasonably accurate. This is the case of the so-called L_1 estimator given by the following minimization [RL87] :

$$\min_{R,t} \sum_k \|r_k\|. \tag{3}$$

Unlike the case of LS estimation, only a numerical solution to equation (3) can be performed. To do so, implementing a gradient descent is difficult since the criterion in equation (3) has a singularity for null residuals. Instead, we can use the Powell's algorithm [PFTV92], which does not manipulate the criterion derivatives. It proved itself to be very efficient in our case. For a displacement field containing 5000 displacement vectors (the maximum size we deal with for aligning histological slices), the computation time required is of the order of one second on a workstation Dec PWS 500au. It is linearly dependent on the field size.

Our experiments have borne out that the L_1 estimator handles outlying displacements much better than LS. However, the outliers still have an influence on the result, even if it is much reduced. This observation encouraged us to improve the L_1 estimator.

At this point, we may notice that the LS and L_1 estimators do not depend on the coordinate system in which the data vectors (x_k, y_k) are given (provided it is orthonormal). This arises from the fact that the criteria minimized in equation (2) and equation (3) depend on the residuals' *Euclidean* norms, $\|r_k\|$. Although this "isotropy" property seems natural, our displacement fields are computed in a way that makes the images axes play a preferential role (see 2.2.1). Hence, there is actually no reason for using an isotropic estimator.

In our case, the authorized displacements between two blocks follow the image pixel grid since they are translations discretised along the image axes (each translation equals to an integer number of pixels). Suppose that two matched blocks are distant from m pixels along the first axis, and n pixels along the second one : if we draw a path *following the image grid* from one block to the other, it cannot have a length lower than $|m| + |n|$, i.e. the 1-norm of the vector with coordinates (m, n) (see Figure 5). This non-Euclidean distance is known as the Manhattan distance.

Based on this intuitive argument, we propose a non-isotropic adaptation of the L_1 estimator, which consists of replacing the residuals' Euclidean norm in

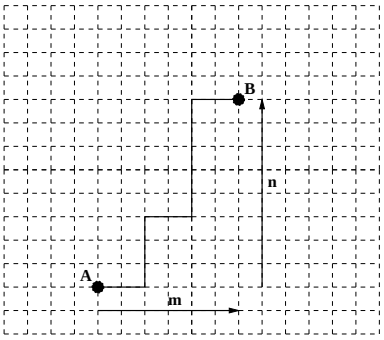

Figure 5: *Manhattan distance.* $|m| + |n|$ *is the minimal length of a path following the grid from point A to point B. Thus, it defines the grid distance between A and B :* $d_{grid}(A, B) = |m| + |n|$.

equation (3) with their 1-norm, yielding :

$$\min_{R,t} \sum_k \|r_k\|_{\mathbf{1}}, \qquad \text{with} \quad \|r_k\|_{\mathbf{1}} = |r_{k,1}| + |r_{k,2}|, \tag{4}$$

where $(r_{k,1}, r_{k,2})$ are the coordinates of the i^{th} residual. In the following, we will denote this estimator L_1^*.

Table 1: *Summary of the estimators presented in section 2.3.*

Acronym	Minimization criterion
LS	$\sum_{k=1}^{n} r_{k,1}^2 + r_{k,2}^2$
L_1	$\sum_{i=k}^{n} \sqrt{r_{k,1}^2 + r_{k,2}^2}$
L_1^*	$\sum_{i=k}^{n} \lvert r_{k,1}\rvert + \lvert r_{k,2}\rvert$

The implementation of L_1^* using Powell's algorithm yields the same computation times as for L_1. However, we have noted experimentally a sensible improvement in the estimation accuracy.

We do not see a rigorous argument to account for the superiority of L_1^* on L_1 in our case. For the time being, we believe that the 1-norm may be

better-adapted to the motion discretization provided by the block matching algorithm, whereas the Euclidean distance should be more adapted to continuous displacements.

2.4 Multi-scale implementation

To obtain the most precise displacement field $\mathcal{D}_{I \to I_1}$, we should choose low values for Δ_1 and Δ_2. The complexity $\mathcal{C}$ to compute the displacement field is the number of tested blocks in I multiplied by the number of compared blocks in I_1 multiplied by the complexity of the similarity measure which is in N^2:

$$\mathcal{C} \propto \left(\frac{X}{\Delta_1} \times \frac{Y}{\Delta_1}\right) \times \left(\frac{2N}{\Delta_2}\right)^2 \times N^2$$

So to reduce the complexity, we must choose a low value for N and large ones for Δ_1 and Δ_2. We propose a multi-resolution method to determine automatically the values of these parameters that lead to accurate the result in a reasonable time. For a high level, we will have a large value for N, Δ_1 and Δ_2. And for a low level, we will decrease N, Δ_1 and Δ_2. In this manner, we find large displacements in the higher levels with a low precision and we refine the solution in the lower levels.

How do we initialize the scale?

We set the multi-scale parameters according to the size of the image. Let N_0 be the initial block size, Δ_1^0 and Δ_2^0 be the initial parameters:

$$N_0 = \min\left(\frac{X, Y}{8}\right) \quad \Delta_1^0 = \frac{N_0}{4} \quad \Delta_2^0 = 4$$

How do we change the scale?

Let k be the multi-scale level. We propose to change the multi-scale parameters:

$$N_k = \max\left(\frac{N_0}{2^k}, 4\right) \quad \Delta_1^k = \max\left(\frac{\Delta_1^0}{2^k}, 1\right) \quad \Delta_2^k = \max\left(\frac{\Delta_2^0}{2^k}, 1\right)$$

When do we decide to change the scale?

At each step of multi-scale, we compute a variation measure δ between the new transformation $S \circ T$ and the old transformation T (see Figure 3). Let $P_1(0,0)$, $P_2(X,0)$, $P_3(0,Y)$, $P_4(X,Y)$ be the four corners of the floating image:

$$\delta = \frac{1}{4} \sum_{i=1}^{4} \|S \circ T(P_i) - T(P_i)\|^2 \tag{5}$$

If δ is inferior to a bound ϵ_k, we decrease the scale level k. Otherwise we reiterate with the same scale. We set $\epsilon_k = \frac{N_k}{8}$ to be consistent with the scale of the transformation. In this manner, the multi-scale scheme is entirely automatic.

What is the new complexity ?

We can now evaluate the complexity of one step at the scale level k depending of the value of Δ_2^k:

$$\mathcal{C}_k \propto \left(\frac{X}{\Delta_1^k} \times \frac{Y}{\Delta_1^k}\right) \times \left(\frac{2N_k}{\Delta_2^k}\right)^2 \times N_k^2$$

$$\begin{cases} \mathcal{C}_k & \propto & 4XYN_0^2 & \text{for} & k \leq 2 \\ \mathcal{C}_k & \propto & 64XY\dfrac{N_0^2}{2^{2k}} & \text{for} & k > 2 \end{cases}$$

So, when we change the scale level to improve the accuracy, the computation time remains stable or decreases.

3 Robustness and accuracy analysis

The aim of this section is to characterize the performances of the algorithm and to determine the robustness of the results with respect to the algorithm parameters. As a ground truth, we use the data of one rat brain from the UCLA rat brain atlas [TSHA95]. In this dataset, the cryoplaned block-face was consistently positioned during sections acquisition to avoid serial image registration. Thus, the "ground truth" registration between consecutive sections is the identity. To test for the performance of the algorithm, we take two consecutive sections and resample one of the section with a known rigid transformation (see Figure 6). Then, we study the error $\delta\theta = |\theta - \hat{\theta}|$ on the rotation

angle and the error $\delta t = \|t - R_\theta \hat{t}\|$ on translation component [PT97]. In the following, experiments are performed on 3 couples of contiguous sections. To speed-up the statistics (we performed more than 1600 registrations...), we extracted a corresponding sub-image of size 256 x 256 in the 1024 x 1024 images. The correlation window size at the higher level is $32 = 256/8$.

Sensitivity to rotation A first experiment with a translation that lower to 40 voxels shows that the algorithm is almost completely insensitive to this kind of translations. Thus, we can focus in a first step on the parameter θ alone.

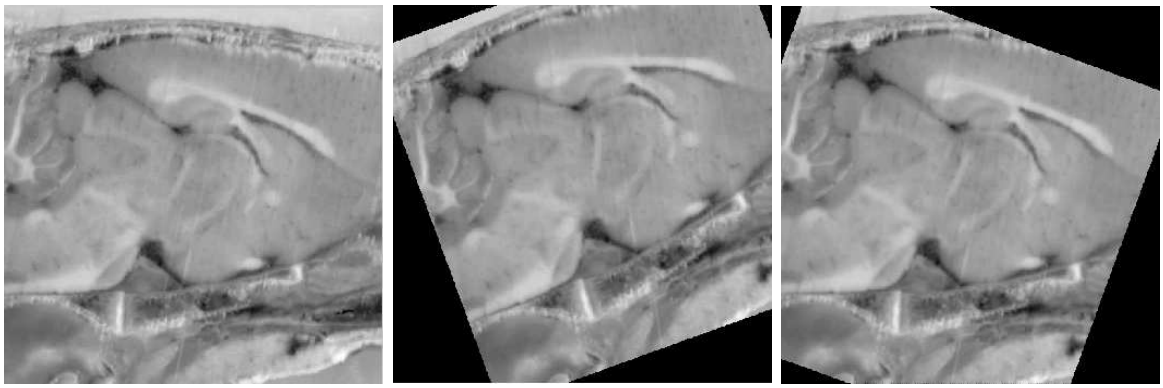

Figure 6: *Left and center: two consecutive slices shifted by a rotation of* 20 *degrees. Right: the second slice is registered to the first one.*

In Figure 7, we show the rotation error δt with respect to the rotation angle θ. Each point on the graph is the average value for 50 registrations with random translations. On the large scale graph, we clearly see that the algorithm always converge for rotations of angle less than $\theta_{\text{cut}} = 28$ deg. For higher values, the algorithm occasionally diverges (or diverges constantly for high values of θ). The second observation (on the small scale graph) is that the mean error (or the accuracy) of the translation is statistically constant when the algorithm converges (here, a RMS of 0.75 voxels). We observed exactly the same type of graphs for the error on the rotation angle, with the same cutting angle value and a mean accuracy of 0.2 degrees.

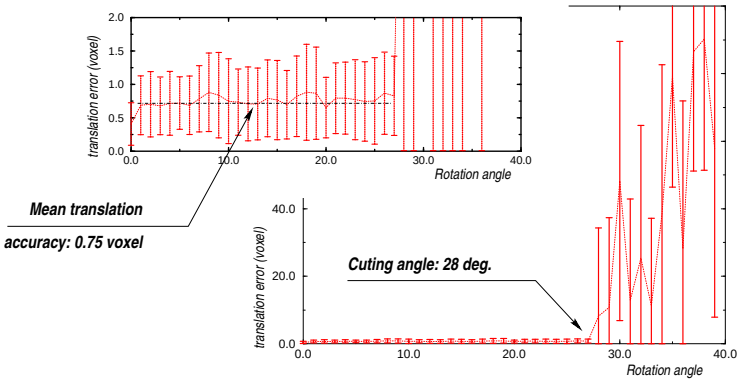

Figure 7: Accuracy of the estimated translation with respect to the angle of rotation.

Sensitivity to translation To study the robustness with respect to the translation norm, we repeated the same experiment as above, but keeping rotations under 15 degrees with a translation range from 0 to 100 voxels. We obtain very similar results: a statistically constant accuracy of the transformation for translations less than a threshold (same mean values as above), and sporadic to continual divergence above this threshold.

Here, the value of the cutting value $\delta t_{\text{cut}} = 52$ voxels is explainable: it corresponds approximately to 1.5 times the size of the correlation window at the higher level (here $N = 32$ voxels). Since the block matching is optimized with a maximal displacements of N, 1.5 times this size means that at least 50 % of the corresponding block should be in the research area, which is in accordance with what we expected. Hence, the size of the convergence basin for translations is directly linked to the window size N and can be extended by taking larger windows.

4 Presentation of the results

Rat's brain

In a first experiment, we have registered 20 sections of rat's brain with a resolution of 768×576 pixels ($0.03 \times 0.03 mm$) and an inter-section gap of $0.4 mm$ (data from Sanofi-Research, Montpellier - France). In Figure 8, we compare the result with the original data and with a classical method based on the principal axes [HH88]. We have a good spatially correlation between the sections as we can see how inner anatomical structures appear. The registration of two sections takes around 2 minutes on a current workstation.

In a second experiment, we were faced to the problem of segmenting an ischemia area that appears lighter in an other set of 26 sections of rat's brain (data from Sanofi-Research, Montpellier - France). A simple thresholding gave a lot of different parts and it was impossible to correlate the parts from one section to another. After the registration, we were able to use 3D digital topology techniques to find the largest connected component corresponding to the ischemia area. Moreover, it is then possible to obtain a 3D reconstruction of the ischemia area as well as the cortical surface and to compute precisely their volumes (see Figure 9). We can compare the result with other 3D rat brain reconstructions (see Figure 10) from UCLA [TSHA95] and from MR data (images from Sanofi-Research, Montpellier - France). Even if in our data, the inter-section was very large and we did not have all the rat's brain, our result appears visually consistent.

Endometrical adenocarcinoma

We have registered 26 sections of an endometrial adenocarcinoma with a resolution of 768×576 pixels ($2.5 \times 2.5 \mu m$) and an inter-section gap of $8 \mu m$ (data from Dr. Christophe Sattonnet, Anatomo-pathology Laboratory, Cagnes-sur-Mer - France). The study of the 3D reconstruction (see Figure 11) allows to show its large complexity and the alternation of the papillar, tubular pattern and solid zones. It also makes possible to evaluate the ratio between the proliferating tissue mass and the adaptive stroma or the conjonctive tissue. This could lead to define quantitative measures useful for the prognosis.

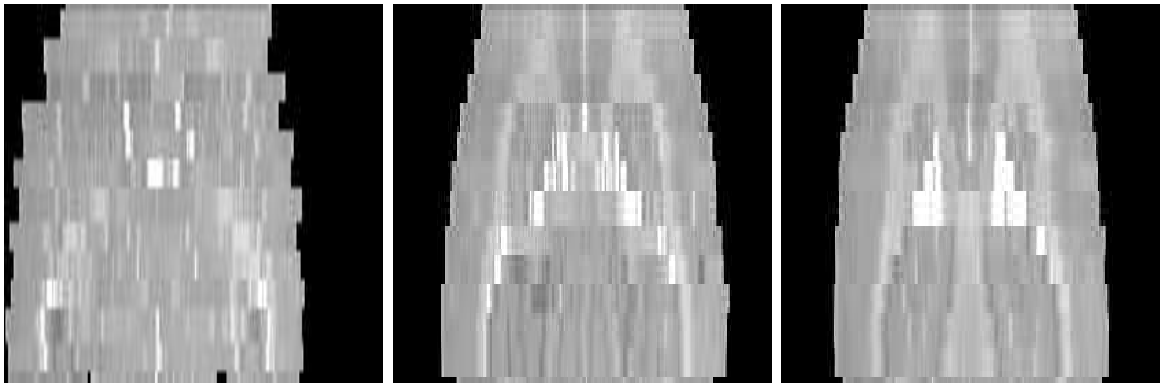

Figure 8: *Median perpendicular view of the section set: left, initial data; middle, after registration with principal axes method and right, after registration with the proposed method.*

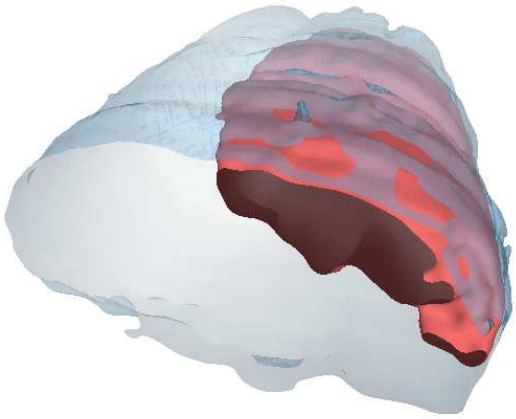

Figure 9: *3D reconstruction with ischemia area segmentation.*

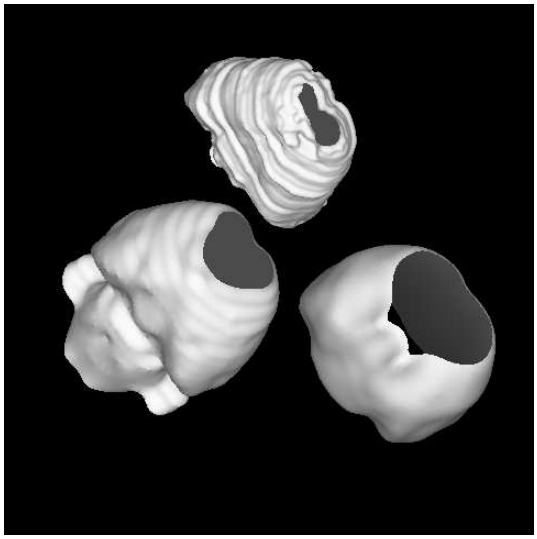

Figure 10: *Up: 3D reconstruction with histological sections. Left: 3D reconstruction with the rat's brain data block available on http://www.loni.ucla.edu/data/index.html. Right: 3D reconstruction from MR images.*

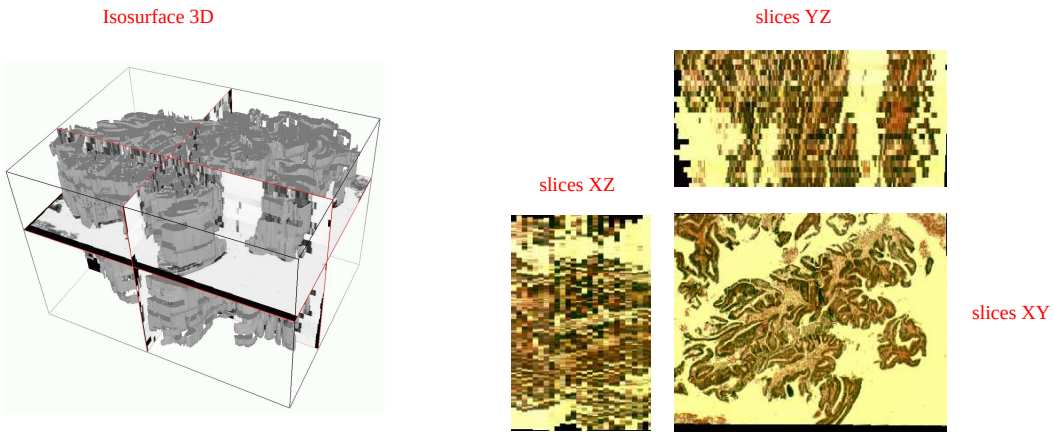

Figure 11: *Right: After registration of histological section. Left: 3D reconstrcution of the endometrical adenocarcinoma.*

5 Future work

In this report, we have presented a new method to align histological sections. We have carefully studied the problem of robustness and we have proposed several ideas to deal with inter-section intensity differences and background artifacts. We have demonstrated experimentally that we can reach a sub-voxel accuracy.

The 3D reconstruction from serial sections may lead to numerous applications both to the microscopic and the macroscopic levels.

At the microscopic level, that corresponds to a magnification larger than 100, the 3D reconstruction study will allow to define new and more accurate histological and cytological parameters as the tumoral angiogenis in oncology, the fibrosis development in hepatitis, the cellular distortions in prion diseases and, more generally to quantify many physiological and pathological phenomena.

At the macroscopic level, the 3D reconstruction study will allow to study objects that are too small to be accurately dissected and too large to be analyzed only based on the 2D slices. In particular, this will make possible to analyze the cardiopathies in foetal-pathological medicine.

In the future, we plan to test the method on other histological data sets containing more sections and with more complex anatomical structures. We also plan to achieve non-rigid registration in order to compensate for geometrical distortions. This algorithm will be tested within the European Research Project QAMRIC to study the Creutzfeldt-Jakob disease (*http://www.inria.fr/epidaure/Collaborations/QAMRIC/qamric.html*).

Acknowledgments

The authors would like to thank Elf and Sanofi-Research, Montpellier - France, Paul Thompson, LONI, UCLA for providing us with data.

References

[ADAL92] A. Andreasen, A.M. Drewes, J.E. Assentoft, and N.E. Larsen. Computer-assisted alignment of standard serial sections without use of artificial landmarks. A practical approach to the utilization of incomplete information of 3-D reconstruction of the hippocample region. *Journal of Neuroscience Methods*, 45:199–207, 1992.

[BK97] V. Bhaskaran and K. Konstantinides. *Image and Video Compression Standards*. KAP, 1997.

[Bro92] G.L. Brown. A Survey of Image Registration Techniques. *ACM Computing Surveys*, 24(4):325–376, 1992.

[CYHN98] F.S. Cohen, Z. Yang, Z. Huang, and J. Nissanov. Automatic Matching of Homologous Histological Sections. *IEEE Transaction on Biomedical Engineering*, 45(5):642–649, 1998.

[DSC+93] M.H. Deverell, J.R. Salisbury, M.J. Cookson, J.G. Holman, E. Dykes, and F. Whimster. Three-dimensional reconstruction: methods of improving image registration and interpretation. *Analytical Cellular Pathology*, 5:253–263, 1993.

[Dum96] E. Dumas. *Recalage IRM-Histologie de cerveau de babouin en 3D*. PhD thesis, Université de Caen - ISMRA, 1996. Rapport de DEA.

[ELF97] D.W. Eggert, A. Lorusso, and R.B. Fisher. Estimating 3D Rigid Body transformations: A Comparison of Four Major Algorithms. *Machine Vision Applications, Special Issue on Performance Characteristics of Vision Algorithms*, 9(5/6):272–290, 1997.

[GTH+95] A.F. Goldszal, O.J. Tretiak, P.J. Hand, S. Bhasin, and D.L. McEachron. Three-dimensionnal Reconstruction of Activated Columns from 2-[14C]Deoxy-D-glucose Data. *Neuroimage*, 2:9–20, 1995.

[HH88] L.S. Hibbard and R.A. Hawkings. Objective image alignment for three-dimensional reconstruction of digital autoradiograms. *Journal of Neuroscience Method*, 26:55–74, 1988.

[KBFM97] B. Kim, J.L. Boes, K.A. Frey, and C.R. Meyer. Mutual Information for Automated Unwarping of Rat Brain Autoradiographs. *Neuroimage*, 5:31–40, 1997.

[KFM+95] B. Kim, K.A. Frey, S. Mukhopadhyay, B.D. Ross, and C.R. Meyer. Co-Registration of MRI and Autoradiography of Rat Brain in Three-Dimensions Following Automatic Reconstruction of 2D Data Set. In N. Ayache, editor, *Computer Vision, Virtual Reality and Robotics in Medicine*, volume 905 of *Lecture Notes in Computer Science*, pages 262–266, Nice (France), 1995. Springer.

[KRBC96] P.A. Kay, R.A. Robb, D.G. Bostwick, and J.J. Camp. Robust 3-D Reconstruction and Analysis of Microstructures from Serial Histologic Sections, with Emphasis on Microvessels in Prostate Cancer. In K. H. Höhne and R. Kikinis, editors, *Visualisation in Biomedical Computing*, volume 1131 of *Lecture Notes in Computer Science*, pages 129–134, Hamburg (Germany), 1996. Springer.

[LM95] Z.-D. Lan and R. Mohr. Robust Matching by Partial Correlation. Technical Report 2643, INRIA, 1995. Electronic version: *http://www.inria.fr/RRRT/RR-2643.html*.

[MCV+97] F. Maes, A. Collignon, D. Vandermeulen, G. Marchal, and P. Suetens. Multimodality Image Registration by Maximization of Mutual Information. *IEEE Transactions on Medical Imaging*, 16(2):187–198, 1997.

[PFTV92] W. H. Press, B. P. Flannery, S. A. Teukolsky, and W. T. Vetterling. *Numerical Recipes in C*. Cambrige University Press, 1992.

[PT97] X. Pennec and J.P. Thirion. A framework for uncertainty and validation of 3D registration methods based on points and frames. *Int. Journal of Computer Vision*, 25(3):203–229, 1997. Electronic version: *http://www.inria.fr/RRRT/RR-2470.html*.

[PWL+98] G.P. Penney, J.W. Weese, J.A. Little, P. Desmedt, D. LG Hill, and D.J. Hawkes. A Comparaison of Similarity Measures for Use in 2D-3D Medical Image Registration. In *First International Conference*

on Medical Image Computing and Computer-Assisted Intervention, volume 1496 of *Lecture Notes in Computer Science*, pages 1153–1161, Cambrdige (USA), October 1998. Springer.

[RCM+97] A. Rangarajan, H. Chui, E. Mjolsness, S. Pappu, L. Davachi, P. Goldman-Rakic, and J. Duncan. A robust point-matching algorithm for autoradiograph alignment. *Medical Image Analysis*, 1(4):379–398, 1997.

[RL87] Peter J. Rousseuw and Annick M. Leroy. *Robust Regression and Outlier Detection*. Wiley Series in Probability and Mathematical Statistics, first edition, 1987.

[RMPA98] A. Roche, G. Malandain, X. Pennec, and N. Ayache. The Correlation Ratio as a New Similarity Measure for Multimodal Image Registration. In *First International Conference on Medical Image Computing and Computer-Assisted Intervention*, volume 1496 of *Lecture Notes in Computer Science*, pages 1115–1124, Cambridge (USA), October 1998. Springer. Electronic version: *http://www.inria.fr/RRRT/RR-3378.html*.

[SB97] G. Simon and M-O. Berger. A two-stage robust statistical method for temporal registration from features of various type. Technical Report 3235, INRIA, 1997. Electronic version: http://www.inria.fr/RRRT/RR-3235.html.

[SZ97] T. Shormann and K. Zilles. Limitation of the Principale-Axes Theory. *IEEE Transactions on Medical Imaging*, 16(6):942–947, 1997.

[TSHA95] A.W. Toga, E.M. Santori, R. Hazani, and K. Ambach. A 3d digital map of rat brain. *Brain Research Bulletin*, 38(1), 1995. Data available at: *http://www.loni.ucla.edu/data/rat/*.

[Vio97] P. Viola. Alignment by Maximisation of Mutual Information. *International Journal of Computer Vision*, 24(2):137–154, 1997.

[ZDFL94] Z. Zhang, R. Deriche, O. Faugeras, and Q-T. Luong. A Robust Technique for Matching Two Uncalibrated Images Through the Recovery of the Unknown Epipolar Geometry. Technical Report 2273,

INRIA, 1994. Electronic version: *http://www.inria.fr/RRRT/RR-2273.html.*

[ZYG93] W. Zhao, T.Y. Young, and M.D. Ginsberg. Registration and Three-Dimensional Reconstruction of Autoradiographic Images by the Disparity Analysis Method. *IEEE Transactions on Medical Imaging*, 12(4):782–791, 1993.

Unité de recherche INRIA Sophia Antipolis
2004, route des Lucioles - B.P. 93 - 06902 Sophia Antipolis Cedex (France)

Unité de recherche INRIA Lorraine : Technopôle de Nancy-Brabois - Campus scientifique
615, rue du Jardin Botanique - B.P. 101 - 54602 Villers lès Nancy Cedex (France)
Unité de recherche INRIA Rennes : IRISA, Campus universitaire de Beaulieu - 35042 Rennes Cedex (France)
Unité de recherche INRIA Rhône-Alpes : 655, avenue de l'Europe - 38330 Montbonnot St Martin (France)
Unité de recherche INRIA Rocquencourt : Domaine de Voluceau - Rocquencourt - B.P. 105 - 78153 Le Chesnay Cedex (France)

Éditeur
INRIA - Domaine de Voluceau - Rocquencourt, B.P. 105 - 78153 Le Chesnay Cedex (France)
http://www.inria.fr
ISSN 0249-6399